

# Variation of magnetic properties of $\text{Sr}_2\text{FeMoO}_6$ due to oxygen vacancies

Martin Hoffmann<sup>1</sup>, Victor N Antonov<sup>2,3</sup>, Lev V Bekenov<sup>2,4</sup>,  
Kalevi Kokko<sup>5,6</sup>, Wolfram Hergert<sup>7</sup> and Arthur Ernst<sup>1,4</sup>

<sup>1</sup> Institute for Theoretical Physics, Johannes Kepler University Linz, Altenberger Straße 69, 4040 Linz, Austria

<sup>2</sup> G. V. Kurdyumov Institute for Metal Physics of the N.A.S. of Ukraine, 36 Vernadsky Street, 03142 Kiev, Ukraine

<sup>3</sup> Faculty of Mathematics and Informatics, University of Białystok, K. Ciolkowskiego 1M, PL-15-245 Białystok, Poland

<sup>4</sup> Max Planck Institute of Microstructure Physics, Weinberg 2, 06120 Halle, Germany

<sup>5</sup> Department of Physics and Astronomy, University of Turku, FIN-20014 Turku, Finland

<sup>6</sup> Turku University Centre for Materials and Surfaces (MatSurf), Turku, Finland

<sup>7</sup> Institute of Physics, Martin Luther University Halle-Wittenberg, Von-Seckendorff-Platz 1, 06120 Halle, Germany

E-mail: [martin.hoffmann@jku.at](mailto:martin.hoffmann@jku.at) and [arthur.ernst@jku.at](mailto:arthur.ernst@jku.at)

Received 19 April 2018

Accepted for publication 11 June 2018

Published 3 July 2018



CrossMark

## Abstract

Oxygen vacancies can be of utmost importance for improving or deteriorating physical properties of oxide materials. Here, we studied from first-principles the electronic and magnetic properties of oxygen vacancies in the double perovskite  $\text{Sr}_2\text{FeMoO}_6$  (SFMO). We show that oxygen vacancies can increase the Curie temperature in SFMO, although the total magnetic moment is reduced at the same time. We found also that the experimentally observed valence change of the Fe ions from 3+ to 2+ in the x-ray magnetic circular dichroism (XMCD) measurements is better explained by oxygen vacancies than by the assumed mixed valence state. The agreement of the calculated x-ray absorption spectra and XMCD results with experimental data is considerably improved by inclusion of oxygen vacancies.

Keywords: oxide, double perovskite, oxygen vacancies, electronic structure, Curie temperature

Supplementary material for this article is available [online](#)

(Some figures may appear in colour only in the online journal)

## 1. Introduction

Double perovskites  $A_2BB'O_6$  ( $A$  = alkaline earth or rare earth metal atoms and  $BB'$  = heterovalent transition metal atoms such as  $B = \text{Fe, Cr, Mn, Co, Ni}$ ;  $B' = \text{Mo, Re, W}$ ) often demonstrate intrinsically complex magnetic structures and a wide variety of physical properties (see [1] for a review article on these materials). In order to understand the complex properties, experiments on SFMO included numerous methods like photoemission spectroscopy (PES) [2–4], Mössbauer spectroscopy [5, 6], neutron scattering [7–9], x-ray absorption spectroscopy (XAS), and x-ray magnetic circular dichroism

(XMCD) measurements [10–12]. Since the XAS and XMCD spectroscopy is very sensitive to the electronic structure and the local environment, comparing calculated spectra to the available experimental results can provide important information about the chemical composition, the ionic valency, and the degree of electronic correlations in the system. Thus, we simulated the XAS and XMCD spectra with our method and found a better agreement than previous density functional calculations [13]. Our results indicate as well a mixed valency of the Fe ion ( $\text{Fe}^{2+}$  or  $\text{Fe}^{3+}$ ) observed by experiments [6, 7, 10, 11], but we can also conclude from our study that the mixed valency is mainly caused by oxygen vacancies.



In addition, several experimental and theoretical studies have demonstrated that the double perovskite system  $\text{Sr}_2\text{FeMoO}_6$  (SFMO) and other related materials exhibit a ferromagnetic (FiM) half-metallic ground state with a high Curie temperature of 324 K to 420 K [14–17]. The physical origin of the magnetoresistance in SFMO is half-metallicity [18], i.e. the material is an insulator in one of the spin channels, but a metal in the other. This leads to a complete spin polarization at the Fermi level, which immediately suggests their application as a source of spin polarized charge carriers in spintronic devices. Therein, SFMO will be used mainly as a thin film, and many attempts were made to grown high quality films [16, 17, 19–21]. But all these films yield a reduced Curie temperature, which is up to 80 K smaller than for bulk samples [16, 17]. Even for bulk SFMO the theoretical magnetic moment of  $4 \mu_B$  was rarely experimentally observed [8]. Such variations were attributed to lattice defects like grain boundaries or point defects. In particular, swapping of Fe and Mo ions, antisite disorder (ASD) [22–28], and oxygen vacancies ( $V_O$ ) [25, 26, 29, 30] were shown to reduce the magnetization of SFMO.

Nevertheless, no study addressed explicitly the variation of the Curie temperature,  $T_C$ , with oxygen vacancies ( $V_O$ ). We deploy therefore the Korringa–Kohn–Rostoker Green’s function (KKR-GF) method with the coherent potential approximation (CPA). We calculated magnetic coupling constants with the magnetic force theorem [31] and used them in a classical Heisenberg model in order to calculate the Curie temperature similarly done as in [32, 33]. A similar approach handling ASD from first-principles was beyond the scope of this work, since the distribution of those antisite defects has to be studied carefully. A simple random distribution might be ruled out by [34] showing a tendency for antiphase patches, which makes the study of the magnetic coupling of antisite defects a work on its own.

In the following section, we describe the lattice structure of SFMO used in our calculations and give details about the calculation techniques. In section 3, we present the XAS and XMCD calculations for the SFMO compound and demonstrate that oxygen vacancies have to be present in SFMO samples. The influence of oxygen vacancies on the electronic structure and magnetic properties is then discussed in section 4.

## 2. Numerical details

For our calculations of SFMO, we adopted the experimentally found double perovskite structure, where the oxygen atoms provide an octahedral environment around the Fe and Mo sites. The  $\text{FeO}_6$  and  $\text{MoO}_6$  octahedra alternate along the three cubic axes, while the Sr atoms occupy the hollow site formed by the corners of the  $\text{FeO}_6$  and  $\text{MoO}_6$  octahedra at the body-centered positions (figure 1).

SFMO was found to be cubic ( $Fm\bar{3}m$ ) in the paramagnetic phase, but changes into a tetragonal-type structure below a critical temperature [9]. The Sr atoms occupy the  $4d$  Wyckoff positions  $(0, 1/2, 1/4)$ . The Fe atoms occupy the  $2a$  Wyckoff pos.  $(0, 0, 0)$  and Mo the  $4d$  Wyckoff pos.  $(0, 0, 1/2)$ . There are two types of oxygen atoms with  $O_z$  at the  $4e$  Wyckoff pos.

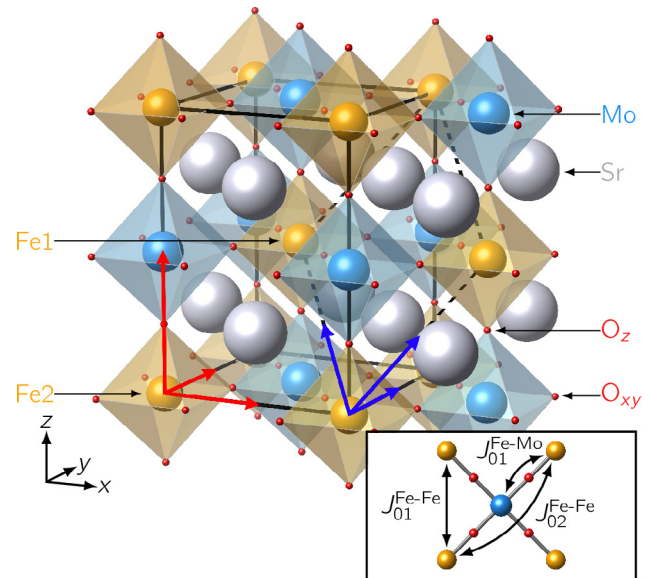


**Figure 1.** The double perovskite structure of SFMO ( $a = b = 5.573$  and  $c = 7.902$  of [36]). The colored polyhedra visualize the octahedral surroundings of the Fe and Mo atoms (orange and blue). Following from the tetragonal symmetry, two different oxygen positions appear (marked with  $O_{xy}$  and  $O_z$ ). The tetragonal supercell is shown by the black solid lines and the red arrows. It contains two functional units with two Fe sites (Fe1, Fe2). The black dashed lines and the blue arrows indicate the primitive unit cell. The inset shows the top view displaying the three most important magnetic coupling pairs between Fe–Fe and Fe–Mo. The figure was prepared with VESTA [39].

$(0, 0, z)$  and  $O_{xy}$  at the  $8h$  Wyckoff pos.  $(x, y, 0)$  (figure 1). Their positions are not definite and vary between different studies. They occupy either the site exactly between Mo and Fe, which gives the body centered tetragonal structure type ( $I4/mmm$ ; No. 139 [35, 36]) or the oxygen octahedra are slightly distorted ( $I4/m$ , No. 87 [37, 38]). We used for simplicity the more symmetric body centered tetragonal structure type and the lattice constant and internal parameters from [36] as input for our study.

We note as well that the slight tetragonal distortion is lifting the degeneracy of the  $d$  states. The crystal field at the Fe (Mo) site (now  $D_{4h}$  point symmetry) splits the Fe (Mo)  $3d$  ( $4d$ ) orbitals into three singlets  $A_{1g}$  ( $d_{3z^2}$ ),  $B_{1g}$  ( $d_{x^2-y^2}$ ), and  $B_{2g}$  ( $d_{xy}$ ) and a doublet  $e_g$  ( $d_{yz}$  and  $d_{xz}$ ). Since the deviation from the ideal  $c/a$  ratio is only small, the states  $d_{xy}$  and  $d_{3z^2}$ , as well as the states  $d_{x^2-y^2}$ ,  $d_{yz}$  and  $d_{xz}$ , form two groups of states, which showed an almost similar density of states (DOS). Those are considered as  $e_g$  and  $t_{2g}$  in accordance with other publications.

For the microscopic understanding of the SFMO compound, we combined the theoretical results of three computational methods, namely the multiple scattering KKR–Green’s function method HUTSEPOT [40, 41], the spin-polarized fully relativistic linear-muffin-tin-orbital (SPR-LMTO) method [42–44] and the Vienna *ab initio* simulation package (VASP) [45, 46]. The main investigation of the electronic and magnetic properties was conducted with HUTSEPOT, whereas the XAS and XMCD spectra were calculated within the SPR-LMTO, and necessary structure relaxations were

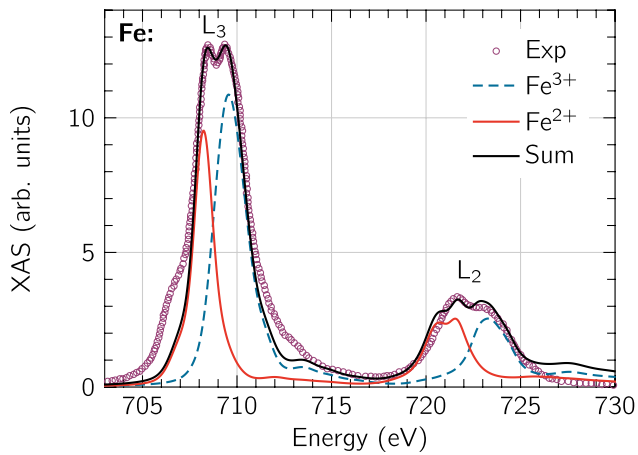


**Figure 2.** The x-ray absorption spectra ([10], open circles) at Fe  $L_{2,3}$  edges as average of left and right circularly polarized light in SFMO measured at 10 K with 5 T magnetic field compared with the theoretically calculated ones for  $\text{Fe}^{3+}$  (dashed blue line) and  $\text{Fe}^{2+}$  (solid red line). The linear combination of 60%  $\text{Fe}^{3+}$  and 40%  $\text{Fe}^{2+}$  denoted as Sum (solid black line) resembles best the reference curve.

achieved with VASP. All relevant input parameters and the discussion about the correct treatment of the electronic structure of SFMO are provided in the supporting information (SI) ([stacks.iop.org/JPhysCM/30/305801/mmedia](http://stacks.iop.org/JPhysCM/30/305801/mmedia)).

### 3. X-ray absorption and XMCD spectra

The valency of the Fe ions is not finally resolved. Experimental studies find a mixed valency state of  $\text{Fe}^{2+}$  and  $\text{Fe}^{3+}$  [6, 7, 10, 11] but theoretical calculations obtain a ground state with  $\text{Fe}^{3+}$  [23, 26, 47]. In order to solve this discrepancy, the x-ray absorption and XMCD spectra at the  $L_{2,3}$  absorption edges can be used in a complex transition metal ionic compound such as SFMO as fingerprints of the ground state.

We used a supercell approximation with a cell of two functional units of SFMO (see red arrows in figure 1). This supercell was relaxed with VASP including a single oxygen vacancy close to Fe2. The relaxation with VASP for a single oxygen vacancy led to a distance of 1.9722 Å between Fe2 and the vacancy—an increase by 1.5%. The correspondent distance between the Fe1 ion and the oxygen vacancy was reduced by 0.5% to 4.4054 Å. In order to crosscheck effects of ASD on the calculated spectra, we included also one antisite defect into the supercell. We found, similarly as in [26], no significant internal relaxations.

The experimentally measured Fe  $L_{2,3}$  absorption spectrum of the SFMO single crystal ([10], average of left and right circularly polarized light) displays at both absorption edges a weak lower-energy shoulder together with a doublet structure at the white line position with almost the same magnitude (figure 2). The complex fine structure of the Fe  $L_{2,3}$  XAS is not compatible with a pure  $\text{Fe}^{3+}$  valency state, since we observed only one peak—similar to [13]—instead of a double peak structure. In order to provide a quantitative description of the spectral features, we took into account both Fe valencies 3+ and 2+, separately, using a primitive unit cell. The theoretically calculated Fe  $L_{2,3}$  XAS agrees most closely with the

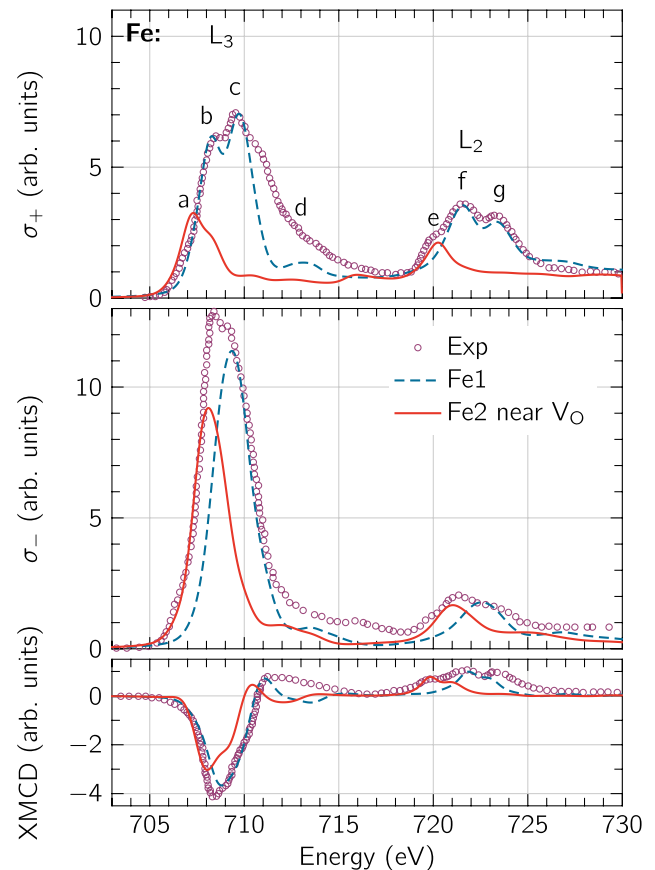


**Figure 3.** The x-ray absorption spectra ([10], open circles) at Fe  $L_{2,3}$  edges in SFMO measured with left ( $\sigma^+$ , top panel) and right circularly polarized light ( $\sigma^-$ , middle panel) measured at 10 K with 5 T magnetic field and XMCD experimental spectrum ([10], lower panel) compared with the theoretically calculated spectra with an oxygen vacancy far away (dashed blue line) and near to an Fe ion (solid red line).

experimental data by using those results in a linear combination of 60%  $\text{Fe}^{3+}$  and 40%  $\text{Fe}^{2+}$  (figure 2), which is opposite to the calculated proportion found in [10] using the framework of the ligand-field atomic formalism.

Considering that the correct Fe valency in the SFMO ground state is 3+ as concluded in many theoretical studies, the mixed valency state might follow again from lattice defects as speculated in [13]. We investigated the influence of the two types of defects in the tetragonal supercell (figure 1). For the antisite defects, we observed only the  $\text{Fe}^{3+}$  solution. This can be connected with the high defect concentration modeled within the supercell. However, a single vacancy among twelve oxygen atoms models a more realistic concentration. Self-consistent calculations in the tetragonal supercell produce the valency of the Fe ions being equal to 2.9+ and 2.4+ at the Fe1 and Fe2 sites, respectively. Therefore, the existence of the vacancy shifts the valency of the nearest Fe ion (Fe2) towards 2+. This valency change could be also observed below in the CPA calculation of the DOS including oxygen vacancies (figure 5).

Indeed, the full explanation of the experimental spectra is only possible by taking into account these crystal imperfections. The Fe  $L_3$  x-ray absorption spectrum for left circularly polarized light ( $\sigma^+$ ) possesses four major fine structures *a*, *b*,

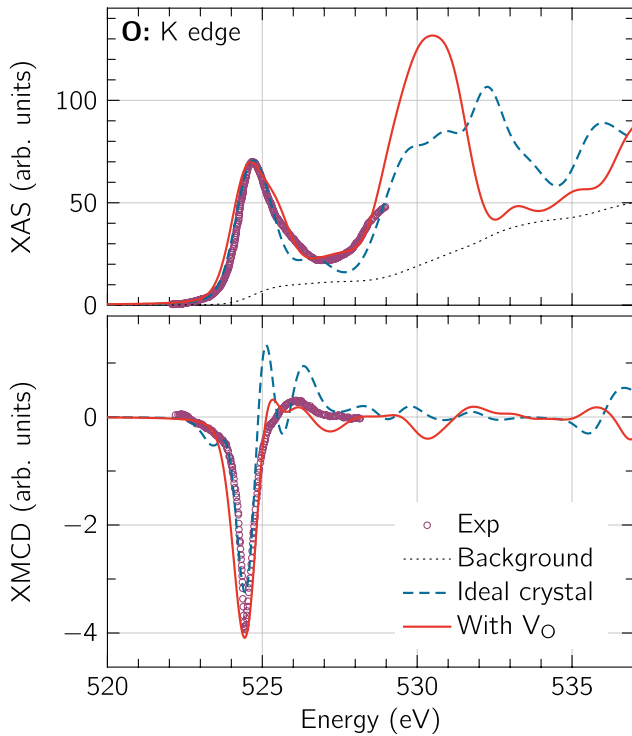


**Figure 4.** The experimental x-ray absorption spectra ([12], open circles) at O  $K$  edge (top panel) in SFMO and experimental XMCD spectra (lower panel) measured at  $T = 20$  K with  $B = 1.1$  T compared with the theoretical simulations carried out for the ideal crystal structure (solid red line) and with an oxygen vacancy (dashed blue line).

$c$  and  $d$  (figure 3). We found that the calculations for the ideal crystal structure with the  $\text{Fe}^{3+}$  ground state solution (dashed blue line) provides the x-ray absorption intensity  $\sigma^+$  only at the major peaks  $b$ ,  $c$ , and  $d$  and do not reproduce the low energy shoulder (peak  $a$ ) as well as the low energy peak  $e$  at the  $L_2$  edge. The calculations with the  $\text{Fe}^{3+}$  solution produce only one high energy peak structure in the  $L_3 \sigma^-$  spectrum (middle panel). However, the experimental measurements exhibit a double-peak structure. The x-ray absorption from the Fe2 atoms with the oxygen vacancy nearby (solid red line) contributes to the low energy peak of  $\sigma^-$  absorption (figure 3). The relative intensity of the peaks depends on the relative concentration of the Fe1 and Fe2 ions in SFMO, in other words, the concentration of defects such as oxygen vacancies. It is similar for the oxygen  $K$  edge. The calculations including an oxygen vacancy are in better agreement with the experimental measurements in the x-ray absorption as well as in the XMCD (figure 4).

The XAS and XMCD spectra at the Mo  $L_{2,3}$  and  $M_{2,3}$  edges are less sensitive for the crystal defects. For both edges, the agreement with the experimental measurements [13] is quite good and independent from the concentration of oxygen vacancies (see SI, figures S4 and S5).

#### 4. Electronic and magnetic properties with randomly distributed oxygen vacancies

We saw above that oxygen vacancies are certainly present in most samples of SFMO. Hence, their impact on electronic and

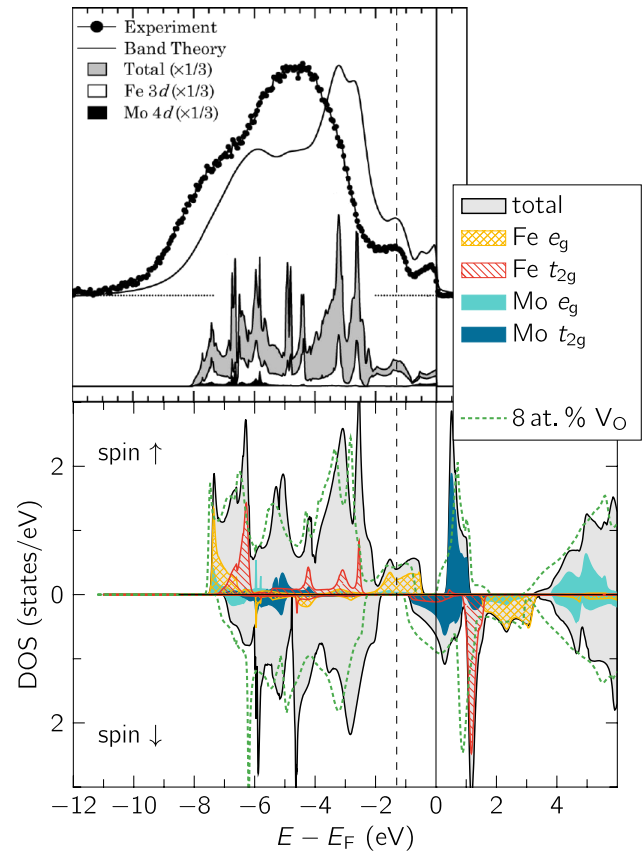


**Figure 5.** The upper panel shows the experimental and simulated PES of SFMO taken as a copy of figure (a) of [2] (some labels were removed). The lower panel represents the DOS for SFMO calculated with the KKR-GF method and  $U_{\text{eff}}^{\text{Fe}} = 2$  eV. The gray area shows the total DOS for defect-free SFMO. The colored regions indicate the LDOS for the  $d$  states of Fe (reddish) and Mo (bluish). The green dotted DOS includes 8 at.% of randomly distributed oxygen vacancies. Both plots are scaled with respect to the same energy scale and the Fermi energy at zero (black vertical line). The dashed line indicates the position of the Fe  $e_g^+$  state in the experimental PES.

magnetic properties should be studied in detail. The KKR-GF method combined with the coherent potential approximation (CPA) allows the study of arbitrary concentrations of randomly distributed oxygen vacancies as done before for  $\text{SrCoO}_{3-\delta}$  [33]. The oxygen vacancies were simulated inside the primitive unit cell with one functional unit of SFMO (see blue arrows in figure 1). The internal lattice positions had to be kept static [36]. We introduced a certain percentage of empty spheres at the lattice sites of the oxygen ions, which are modeled as randomly distributed via CPA. The typical oxygen-deficiency  $\delta$  ranges between 0.006 to 0.36 [24, 29, 48]. This represents 0.1 at.% to 6 at.% of the total oxygen amount in defect-free SFMO.

We obtained for defect-free SFMO the half-metallic ground state by applying correlation corrections following [26, 47, 49] (figure 5). Although the half-metallic ground state would be well represented within the self-interaction correction (SIC) [47], the Fe  $d$  states localize too much. Hence, we applied an  $U$  parameter on the  $d$  states of Fe with  $U_{\text{eff}}^{\text{Fe}} = 2$  eV as a compromise, because we are aware that the correct

**Table 1.** The calculated spin  $m_s$  and orbital  $m_o$  magnetic moments (in  $\mu_B$ ) of Fe and Mo in defect-free SFMO compared with the measured magnetic moments. Experimental uncertainties are given as well.

Method	Fe		Mo	
	$m_s$	$m_o$	$m_s$	$m_o$
SPR-LMTO	4.104	0.041	-0.504	0.047
KKR-GF	3.921		-0.525	
Besse <i>et al</i> [10] <sup>a</sup>	3.05 ± 0.20	0.02 ± 0.02	-0.32 ± 0.05	-0.05 ± 0.05
Koide <i>et al</i> [12] <sup>a</sup>	2.80 ± 0.30	0.093 ± 0.010	-0.36 ± 0.03	-0.037 ± 0.015
García-Landa <i>et al</i> [8] <sup>b</sup>	4.1 ± 0.1		0.0 ± 0.1	
Kanchana <i>et al</i> [13] <sup>c</sup>	3.72	0.042	-0.29	0.020
Fang <i>et al</i> [53] <sup>c</sup>	3.97		-0.39	

<sup>a</sup> XMCD measurement.<sup>b</sup> Neutron diffraction experiment.<sup>c</sup> Theory.

treatment of the electronic structure is very sensitive to the structural [23] and methodological differences [18, 28, 50] (see SI). Following optical [51] and photoemission spectroscopy (PES) [2–4] measurements, the band gap should be 0.5 eV to 1.3 eV, and should open between the Mo  $t_{2g}^{\uparrow}$  states and the Fe  $e_g^{\uparrow}$  states.

Of course, a direct comparison of calculated DOS and experimental spectra is very complicated, since thermal broadening and defect levels can easily reduce the ideal band gap. Saitoh [2] noticed for example possible ASD in their samples (up to 10 at.%) but could not account for defects in their theoretical interpretation. ASD inside SFMO deteriorate the DOS at the Fermi energy  $E_F$  because new states appear in the majority spin channel [23, 25, 26, 28] and reduce the spin polarization, which was indeed observed experimentally [52]. In contrast, a low concentration of oxygen vacancies does not alter the half-metallic character of SFMO [25, 26, 30], but additional Fe  $d^{\downarrow}$  and Mo  $d^{\downarrow}$  states become occupied [26]. This indicates a lower valency of the Fe and Mo ions. Electrons of the removed oxygen atoms occupy states of Fe and Mo ions. A similar qualitative behavior was observed within our calculations of oxygen-deficient SFMO with CPA (green dashed line in figure 5). The averaging within the CPA broadens all states.

Even more interesting is the effect of oxygen vacancies on the magnetic properties of SFMO. As a starting point, we compare briefly the numerically obtained magnetic properties for defect-free SFMO with measured results and introduce then oxygen vacancies again. The expected ferrimagnetic (FiM) ground state of defect-free SFMO was always energetically favorable when comparing possible magnetic configurations. The Fe spin and orbital moments in FiM are parallel, whereas the spin and orbital Mo moments are antiparallel to each other, in accordance with Hund's third rule (table 1). We obtain a good agreement for the orbital Fe magnetic moment (0.041  $\mu_B$ ) with the FPLMTO result of Jeng and Guo [54] (0.043  $\mu_B$ ) and the LMTO results of Kanchana [13] (0.042  $\mu_B$ ). The calculated spin and orbital moments of the Mo atom are always larger in comparison with earlier calculations [13, 18, 53–55]. Also, the Fe spin moment of  $\approx 4 \mu_B$  is in a good agreement with the experimental neutron diffraction

measurements [8] and the theoretical ideal value for the Fe<sup>3+</sup>/Mo<sup>5+</sup> or Fe<sup>2+</sup>/Mo<sup>6+</sup> valency configuration (table 1). However, typical values for the magnetization reported in experimental studies are smaller than  $\approx 4 \mu_B$ . This reduction was always attributed to point defects [10, 22, 29, 56].

We used the CPA to simulate randomly distributed defects and indeed an almost linear decrease of the total magnetic moment agreeing qualitatively with an experimental study by Kircheisen [29] was observed (figure 6(b)). The offset of the measurement at  $\delta = 0$  will result from other point defects like ASD [22]. Surprisingly, the Curie temperature is increasing with more oxygen vacancies, while the total magnetic moment is reduced at the same time (figure 6(b)). We obtained the Curie temperature  $T_C$  by calculation of the magnetic exchange interactions  $J_{ij}$  and consider them up to a distance of 12.49 Å in a Monte Carlo simulation with a classical Heisenberg model [32]. Those results agree also with the mean-field approximation (MFA) or the random-phase approximation (RPA) considering that MFA usually overestimates  $T_C$ .

Although  $T_C$  for defect-free SFMO is below the range of experimental values 324 K to 420 K, we are interested in the relative variation of  $T_C$  with the amount of oxygen vacancies, which is roughly +15 K per at.% of oxygen vacancies. Experimental results might therefore be enhanced by tens of kelvin due to oxygen vacancies.

The reasons for this increase in  $T_C$  can be understood from the magnetic exchange interactions. The most prominent coupling constants of the order of several meV have only a very restricted range up to 7.9 Å (figure 6(a)). This includes only the interactions up to the next nearest neighbor Fe ions  $J_{02}^{\text{Fe-Fe}}$  (see inset in figure 1). Due to the tetragonal structure, all magnetic exchange interactions show a small asymmetry with respect to those with a component in  $z$  direction. For clarity, only the coupling constants in the  $x$ - $y$ -plane are shown (figure 6(a)).

The calculations of  $J_{ij}$  were performed in the FiM reference state. We observe for defect-free SFMO a strong antiferromagnetic (AFM) coupling between Fe and Mo ions and a ferromagnetic coupling between nearest neighbor Fe-Fe,  $J_{01}^{\text{Fe-Fe}}$ . The next nearest Fe-Fe coupling constants,  $J_{02}^{\text{Fe-Fe}}$ , have also an AFM character but are not enough to destabilize the FiM ground state of SFMO (see figure 6(a) for  $\delta = 0$ ).

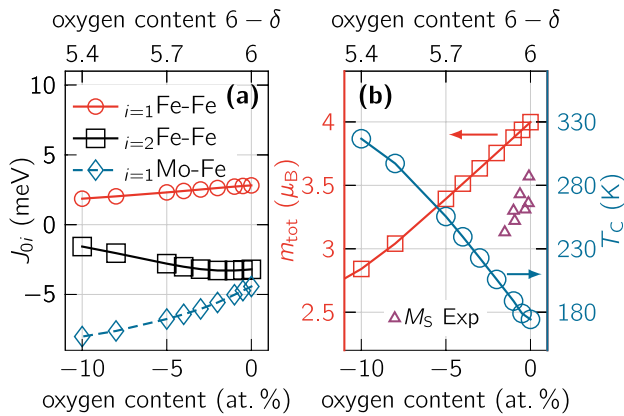


**Figure 6.** Calculated magnetic properties depending on the oxygen deficiency  $\delta$  obtained with the KKR-GF method. (a) Magnetic exchange coupling constants for the strongest interactions (displayed in the inset in figure 1). (b) Total magnetic moment  $m_{tot}$  obtained within the self-consistent calculations and Curie temperatures from the Monte Carlo simulation. Experimental results [29] are given for the saturation magnetization (in  $\mu_B$ ).

Introducing now the oxygen vacancies in a random fashion reduces the oxygen mediated exchange between the Fe ions but favors the AFM exchange between Fe and Mo ions (figure 6(a)). This behavior resembles a stronger orbital localization as observed with an increase of electron correlation parameter  $U_{eff}^{Fe}$  (see SI). The stronger localization of the orbitals leads to a decrease of the electron hopping and, thereby, to a decrease in the magnetic coupling strength. Together, the total magnetic moment will indeed be reduced but the stronger AFM coupling between Fe and Mo sites will at the same time mediate an additional FM coupling and increases  $T_C$ .

## 5. Conclusions

We focused our study on the impact of oxygen defects on the magnetic properties of SFMO and made two crucial findings:

Our simulated x-ray absorption spectra (XAS) and x-ray magnetic circular dichroism spectra (XMCD) show a better agreement with experimental spectra [6, 7, 10, 11] than previous density functional calculations [13]. This indicates that the experimentally observed mixed valency of the Fe ion ( $Fe^{2+}$  or  $Fe^{3+}$ ) is mainly caused by oxygen vacancies.

Second, we could explain the experimentally observed reduction of the total magnetic moment of SFMO by an increasing amount of oxygen vacancies following from a variation of the FM and AFM magnetic coupling between the Fe and Mo ions. At the same time, the Curie temperature shows a strong increase of roughly +15 K per at.% of oxygen vacancies.

Since the growing conditions of SFMO samples could be influenced by the oxygen partial pressure, oxygen vacancies could be a tool to improve the magnetic properties of SFMO, in particular, because the half-metallic band gap is not influenced by oxygen vacancies.

## Acknowledgments

This publication was funded by the German Research Foundation within the Collaborative Research Centre 762 (projects A4 and B1). The support of the German Academic Exchange Service by grant ‘Electronic properties of thin SFMO films’ (grant number 57071667) is greatly acknowledged.

## ORCID iDs

Martin Hoffmann <https://orcid.org/0000-0002-8426-725X>  
 Kalevi Kokko <https://orcid.org/0000-0002-4039-2745>  
 Wolfram Hergert <https://orcid.org/0000-0003-0912-0546>

## References

- [1] Serrate D, De Teresa J M and Ibarra M R 2007 *J. Phys.: Condens. Matter* **19** 23201
- [2] Saitoh T, Nakatake M, Kakizaki A, Nakajima H, Morimoto O, Xu S, Moritomo Y, Hamada N and Aiura Y 2002 *Phys. Rev. B* **66** 035112
- [3] Kang J S *et al* 2002 *Phys. Rev. B* **66** 113105
- [4] Kim J H *et al* 2003 *J. Korean Phys. Soc.* **43** 416 (<http://jkps.or.kr/journal/view.html?uid=5741&vmd=Full>)
- [5] Sarma D D, Sampathkumaran E V, Ray S, Nagarajan R, Majumdar S, Kumar A, Nalini G and Guru Row T N 2000 *Solid State Commun.* **114** 465
- [6] Lindén J, Yamamoto T, Karppinen M, Yamauchi H and Pietari T 2000 *Appl. Phys. Lett.* **76** 2925
- [7] Kapusta Cz, Riedi P C, Zajac D, Sikora M, De Teresa J M, Morellon L and Ibarra M R 2002 *J. Magn. Magn. Mater.* **242–5** 701
- [8] García-Landa B, Ritter C, Ibarra M R, Blasco J, Algarabel P A, Mahendiran R and García J 1999 *Solid State Commun.* **110** 435
- [9] Moritomo Y, Xu S, Machida A, Akimoto T, Nishibori E, Takata M, Sakata M and Ohoyama K 2000 *J. Phys. Soc. Japan* **69** 1723
- [10] Besse M *et al* 2002 *Europhys. Lett.* **60** 608
- [11] Kuepper K, Balasz I, Hesse H, Winiarski A, Prince K C, Matteucci M, Wett D, Szargan R, Burzo E and Neumann M 2004 *Phys. Status Solidi a* **201** 3252
- [12] Koide T, Sekine T, Miyauchi H, Manaka H, Asakura D, Fujimori A, Kobayashi K I, Tomioka Y, Kimura T and Tokura Y 2014 *J. Phys.: Conf. Ser.* **502** 12003
- [13] Kanchana V, Vaitheeswaran G, Alouani M and Delin A 2007 *Phys. Rev. B* **75** 220404
- [14] Kato H, Okuda T, Okimoto Y, Tomioka Y, Oikawa K, Kamiyama T and Tokura Y 2004 *Phys. Rev. B* **69** 184412
- [15] Rubi D, Navarro J, Fontcuberta J, Izquierdo M, Avila J and Asensio M 2006 *J. Phys. Chem. Solids* **67** 575
- [16] Paturi P, Metsänoja M and Huhtinen H 2011 *Thin Solid Films* **519** 8047
- [17] Saloaro M, Deniz H, Huhtinen H, Palonen H, Majumdar S and Paturi P 2015 *J. Phys.: Condens. Matter* **27** 386001
- [18] Kobayashi K I, Kimura T, Sawada H, Terakura K and Tokura Y 1998 *Nature* **395** 677
- [19] Venimadhav A, Sher F, Attfield J and Blamire M 2004 *J. Magn. Magn. Mater.* **269** 101

- [20] Westerburg W, Reisinger D and Jakob G 2000 *Phys. Rev. B* **62** R767
- [21] Kumar D and Kaur D 2010 *Physica B* **405** 3259
- [22] Ogale A S, Ogale S B, Ramesh R and Venkatesan T 1999 *Appl. Phys. Lett.* **75** 537
- [23] Solov'yev I V 2002 *Phys. Rev. B* **65** 144446
- [24] Colis S, Stoeffler D, Mény C, Fix T, Leuvrey C, Pourroy G, Dinia A, Panissod P and Meny C 2005 *J. Appl. Phys.* **98** 033905
- [25] Stoeffler D and Colis S 2005 *J. Phys.: Condens. Matter* **17** 6415
- [26] Muñoz García A B, Pavone M and Carter E A 2011 *Chem. Mater.* **23** 4525
- [27] Erten O, Meetei O N, Mukherjee A, Randeria M, Trivedi N and Woodward P 2011 *Phys. Rev. Lett.* **107** 257201
- [28] Reyes A M, Arredondo Y and Navarro O 2016 *J. Phys. Chem. C* **120** 4048
- [29] Kircheisen R and Töpfer J 2012 *J. Solid State Chem.* **185** 76
- [30] Wu H, Ma Y, Qian Y, Kan E, Lu R, Liu Y, Tan W, Xiao C and Deng K 2014 *Solid State Commun.* **177** 57
- [31] Liechtenstein A I, Katsnelson M I, Antropov V P and Gubanov V A 1987 *J. Magn. Magn. Mater.* **67** 65
- [32] Fischer G, Däne M, Ernst A, Bruno P, Lüders M, Szotek Z, Temmerman W M and Hergert W 2009 *Phys. Rev. B* **80** 014408
- [33] Hoffmann M, Borisov V S, Ostanin S, Mertig I, Hergert W and Ernst A 2015 *Phys. Rev. B* **92** 094427
- [34] Meneghini C, Ray S, Liscio F, Bardelli F, Mobilio S and Sarma D D 2009 *Phys. Rev. Lett.* **103** 046403
- [35] Park S I, Ryu H J, Kim S B, Lee B W and Kim C S 2004 *Physica B* **345** 99
- [36] Burzo E, Balasz I, Valeanu M and Pop I G 2011 *J. Alloys Compd.* **509** 105
- [37] Nakamura S and Oikawa K 2003 *J. Phys. Soc. Japan* **72** 3123
- [38] Azad A K, Eriksson S G, Khan A, Eriksson A and Tsegai M 2006 *J. Solid State Chem.* **179** 1303
- [39] Momma K and Izumi F 2011 *J. Appl. Crystallogr.* **44** 1272
- [40] Lüders M, Ernst A, Temmerman W M, Szotek Z and Durham P J 2001 *J. Phys.: Condens. Matter* **13** 8587
- [41] Lüders M, Ernst A, Däne M, Szotek Z, Svane A, Ködderitzsch D, Hergert W, Györfly B L and Temmerman W M 2005 *Phys. Rev. B* **71** 205109
- [42] Andersen O K 1975 *Phys. Rev. B* **12** 3060
- [43] Nemoshkalenko V V, Krasovskii A E, Antonov V N, Antonov V I N, Fleck U, Wonn H and Ziesche P 1983 *Phys. Status Solidi B* **120** 283
- [44] Antonov V N, Perlov A Ya, Shpak A P and Yaresko A N 1995 *J. Magn. Magn. Mater.* **146** 205
- [45] Blöchl P E 1994 *Phys. Rev. B* **50** 17953
- [46] Kresse G and Joubert D 1999 *Phys. Rev. B* **59** 1758
- [47] Szotek Z, Temmerman W M, Svane A, Petit L and Winter H 2003 *Phys. Rev. B* **68** 104411
- [48] Yamamoto T, Liimatainen J, Lindén J, Karppinen M and Yamauchi H 2000 *J. Mater. Chem.* **10** 2342
- [49] Stoeffler D and Etz C 2006 *J. Phys.: Condens. Matter* **18** 11291
- [50] Sarma D D, Mahadevan P, Saha-Dasgupta T, Ray S and Kumar A 2000 *Phys. Rev. Lett.* **85** 2549
- [51] Tomioka Y, Okuda T, Okimoto Y, Kumai R, Kobayashi K I and Tokura Y 2000 *Phys. Rev. B* **61** 422
- [52] Panguluri R P, Xu S, Moritomo Y, Solov'yev I V and Nadgorny B 2009 *Appl. Phys. Lett.* **94** 012501
- [53] Fang Z, Terakura K and Kanamori J 2001 *Phys. Rev. B* **63** 180407
- [54] Jeng H T and Guo G Y 2003 *Phys. Rev. B* **67** 094438
- [55] Saha-Dasgupta T and Sarma D D 2001 *Phys. Rev. B* **64** 064408
- [56] Balcells L, Navarro J, Bibes M, Roig A, Martínez B and Fontcuberta J 2001 *Appl. Phys. Lett.* **78** 781